JPEDAV (2005) 26:5-19
DOI: 10.1361/15477030522437
1547-7037/$19.00 ©ASM International

Review Paper

Crystallography and Phase Equilibria A Review: Part III—Second-Order Transitions and Approximations

J.F. Smith

(Submitted November 8, 2004)

1. Introduction

In this third part of the review of the relevance of crystallography to phase equilibria, the distinction between first-order and second-order transitions is the first item to be considered. In a first-order transition $\delta G/\delta\xi$ is discontinuous; however, in a second-order transition $\delta G/\delta\xi$ is continuous, but $\delta^2 G/d\xi^2$ is discontinuous. Here G is the Gibbs energy and ξ is a state variable such as temperature, pressure, or composition (T, P, or X). Plots of G versus T are shown in Fig. III-1 to illustrate the difference between first- and second-order transitions. In Fig. III-1(a), the curve for the α-symmetry structure crosses the curve for the β-symmetry structure at a point where the Gibbs energies are the same, but the slopes of the two curves are different, $dG^{\alpha}/dT \neq dG^{\beta}/dT$. The juncture is the transition temperature, T_t. It is obvious that α has the lower Gibbs energy at $T < T_t$ and is the stable structure below T_t, while for $T > T_t$ β has the lower Gibbs energy and is the stable structure. At T_t the two phases can exist in a two-phase equilibrium. Since $dG^i/dT = -S^i$, it is also obvious that $\Delta_i S$ is not zero. Thus, the combination of $\Delta_i G = 0$ and $\Delta_i S \neq 0$ characterizes a first-order transition with two distinct phases in equilibrium at T_t.

For comparison Fig. III-1(b) illustrates the G versus T behavior of a second-order reaction. In this figure, the α- and β-symmetry structures have Gibbs energies that differ at low temperatures but merge at a point where both $G^{\alpha} = G^{\beta}$ and $dG^{\alpha}/dT = dG^{\beta}/dT$ and at temperatures above the merger point, the symmetry difference disappears and the Gibbs energies are indistinguishable. The transition temperature is the point of merger. Figure III-1(b) characterizes a second-order transition, and there is no phase change but rather a transition between two symmetries of the same single phase. The second-order transition contrasts with the first-order transition in that both $\Delta_t G$ and $\Delta_t S$ equal zero in the second-order transition. The symmetries of the two structures in a second-order transition are related in a manner that allows the possibility of the structures to continuously change from one to the other.

The specific conditions that must apply before a second-order transition can occur were first delineated by Landau and Lifshitz[1] on the mathematical basis of group theory. Their result in the language of group theory necessitates that all of four conditions apply:

- Space groups of the structures in a second-order transition must be in a group-subgroup relationship.
- The difference between the particle density functions of the two structures must be a basis function, or combination of basis functions, of the irreducible representation of the higher-symmetry space group.
- It must not be possible to form a totally symmetric third-order combination of such basis functions.
- The low-symmetry structure must be locked in by symmetry to the high-symmetry space group (even if incommensurate).

In a quite readable review of the topic, Franzen[2] discussed the details of the group theoretical treatment and some of the thermodynamic aspects. At this point, it may be noted that nothing in group theory states that the curve in Fig. III-1(b) might not be inverted end-to-end with a single high-symmetry structure at low temperatures, diverging from the high-symmetry form to a low-symmetry form at high temperatures. However, thermodynamic considerations indicate that entropy increases with increasing temperature, and thus the high-symmetry structure should be the form at higher temperature with the low-symmetry structure occurring at temperatures below T_t. The curve as drawn in Fig. III-1(b) is therefore the correct configuration.

For the author and for the many who are not experts in the mathematical formalism of group theory, the statement of conditions in the language of group theory sounds formidable. Therefore, some paraphrasing seems to be in order with the following being implicit in the rules:

- The Landau rules indicate that all symmetry elements of the low-symmetry structure must be present in the high-symmetry structure.
- At constant composition, the loci of the particles (atoms) within the two structures must be definably related.
- There must be no third-order or other odd-order terms in defining the Gibbs energy difference between the structures of the two symmetries.
- It must be possible for the transformation between the high- and low-symmetry structures to occur via a continuous path.

With these conditions in mind, a second-order transition may occur with a change of symmetry at a definable thermodynamic state during a continuous structure change through that state. Such changes may be of three types:

J.F. Smith, J.F. Smith Consulting Services, 2919 S Riverside Dr., Ames, IA 50010. Contact e-mail: jfsmith@iastate.edu.

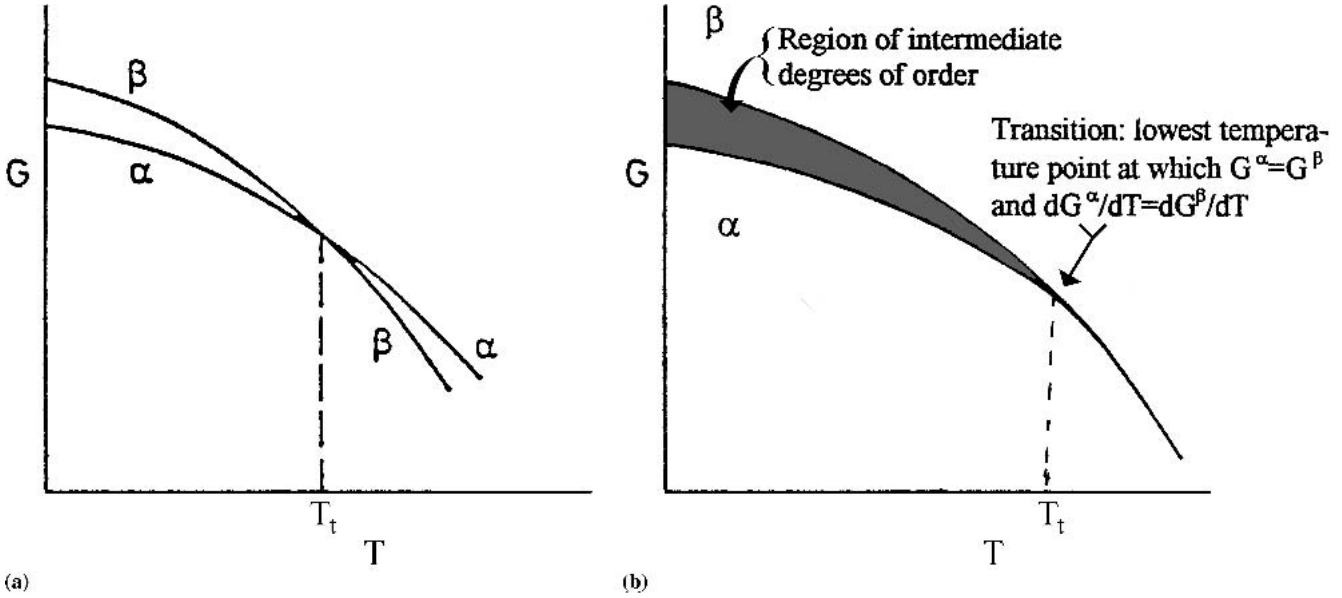

Fig. III-1 Comparison of Gibbs energies versus temperature for first- and second-order transitions. (a) First-order transition; it is shown in the text that at the transition point $\Delta_t G = 0$, while $\Delta_t H = T\Delta_t S \neq 0$, there are two distinct phases. (b) Second-order transition with the text showing that at the transition point $\Delta_t G = \Delta_t H = \Delta_t S = 0$ and the behavior is that of a single phase existing in two different symmetry configurations

- Order-disorder
- Displacive
- A combination of order-disorder and displacive

The β-brass transition that was noted in Part I (*J. Phase Equilibria*, Vol 25 (No. 5), 2004) of this review is an example of an order-disorder transition while the structural changes in $Ni_{10}Zr_7$ noted in Part II (*J. Phase Equilibria*, Vol 25 (No. 6), 2004) of this review is an example of a displacive second-order transition. The ordering change of electric dipoles in $NaNO_2$ is an example of a combined order-disorder, displacive transition.[3] Additional comments concerning these transitions are deferred until later.

2. Thermodynamic Comparison of First- and Second-Order Reactions

A further comparison of first-order and second-order transitions can be made in the following way. For this comparison, a first-order transition is chosen as a transition between two symmetries that are so related that a continuous path could change one symmetry into the other. This choice is, of course, a requirement for a second-order transition but not for a first-order transition. While there are first-order transitions that are not related by a continuous path (e.g., a transition involving nucleation and growth), the choice of a first-order transition with a continuous path between the competing symmetry structures allows the expression of the Gibbs energies of the competing symmetry forms in each type of transition to be expressed in similar form in terms of symmetry-breaking parameters. A simple example of a symmetry-breaking parameter, η, is the one that might be used for the stoichiometric β-brass transition, $\eta = 2f_{Cu} - 1$, where f_{Cu} is the probability of occupancy of the origin site of the unit cell by a Cu atom. Note that since f_{Cu} varies between 1 and 0, η varies between 1 and −1 with random occupancy occurring at $f_{Cu} = 0.5$ and $\eta = 0$. In the case of displacive transitions, one could define η in terms of the fraction of maximum displacement that can occur.

With a continuous gradation between competing symmetry forms, one can expand the Gibbs energy in the vicinity of the transition about the Gibbs energy G° at the transition point in terms of an appropriate symmetry-breaking parameter η. A Taylor expansion of the Gibbs energy around G° in terms of η produces:

$$G = G^\circ + (\delta G/\delta\eta)\eta + (\tfrac{1}{2})(\delta^2 G/\delta\eta^2)\eta^2 + (\tfrac{1}{6})(\delta^3 G/\delta\eta^3)\eta^3 + (\tfrac{1}{24})(\delta^4 G/\delta\eta^4)\eta^4 + \ldots (1/n!)(\delta^n G/\delta\eta^n)\eta^n \quad \text{(Eq 1a)}$$

where G is the Gibbs energy of the low-symmetry structure and G° is the Gibbs energy at the point of equality of the Gibbs energy of the high- and low-symmetry structures. Because the points of interest are the points of minimal Gibbs energy and $\delta G/\delta\eta = 0$ is a necessary condition to define a minimum, the first power term disappears and Eq 1(a) may be rewritten to fourth order as:

$$G = G^\circ + A\eta^2 + B\eta^3 + C\eta^4 \quad \text{(Eq 1b)}$$

With arbitrarily selected coefficients, G-G° in this equation can be plotted as a function of η, as shown in Fig. III-2(a).

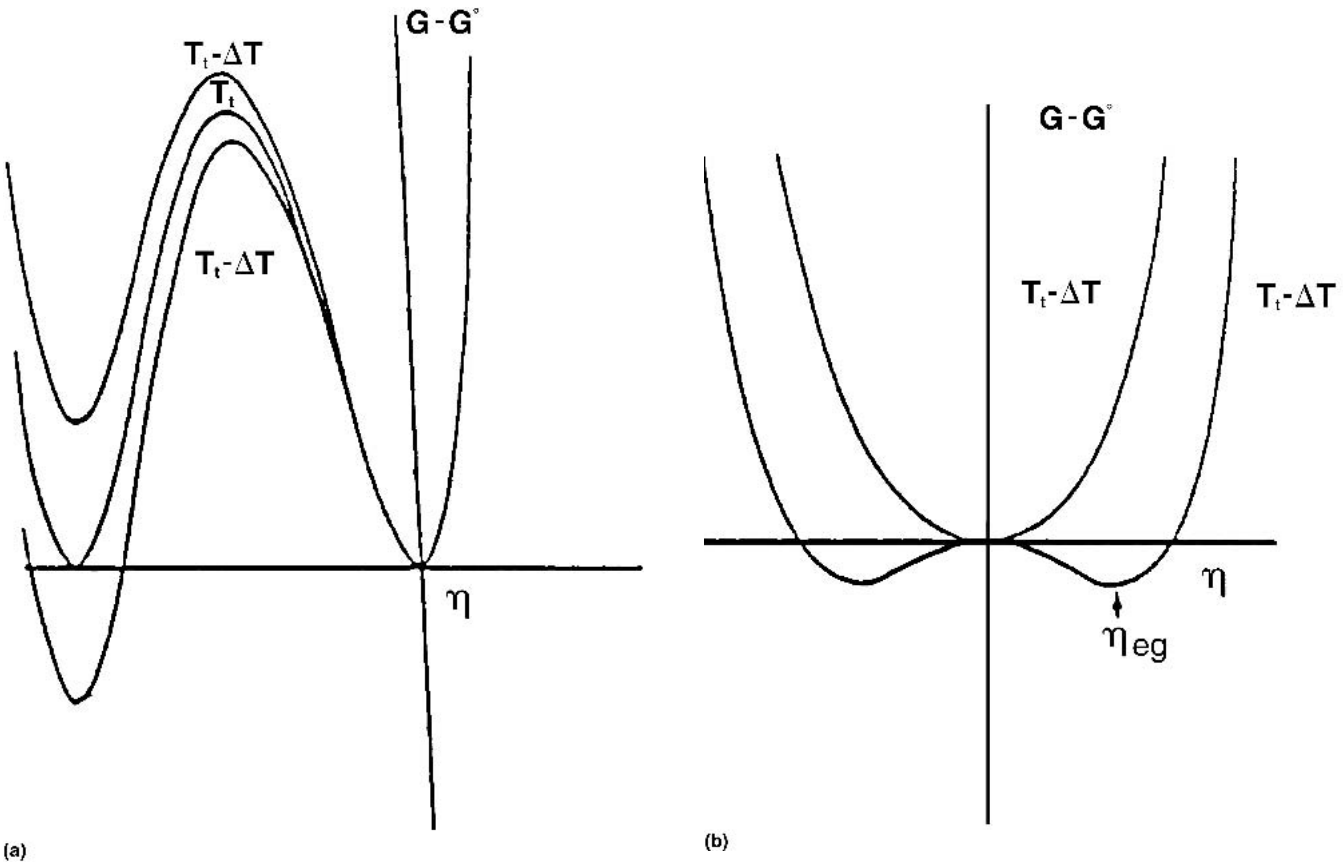

Fig. III-2 Comparison of Gibbs energy differences, G-G° versus η, where G is the Gibbs energy of the low-symmetry structure and G° is the Gibbs energy of the high-symmetry structure. (a) For a first-order transition: the upper curve for $T > T_t$ shows the low-temperature form to be metastable and the high-temperature form to be stable; the middle curve for $T = T_t$ shows the two forms to exist in equilibrium; and the lower curve for $T < T_t$ shows the high-temperature form to be metastable and the low-temperature form to be stable. (b) The situation for a second-order transition: the upper curve shows that for $T = T_t$ and for $T > T_t$ there is a single structure; at $T < T_t$ a double-valued curve develops with minima values of η increasing and of G-G° becoming more negative with decreasing temperature. η of the double-valued curve defines a single symmetry independently of the + or − sign (see text).

Equilibria between the high- and low-symmetry structures will occur when G-$G^\circ = 0$, so Eq 1(b) must be solved for values of η that produce G-$G^\circ = 0$. Obviously $\eta = 0$ is one such solution. Other solutions can be obtained for G-$G^\circ = 0$ by converting:

$$A\eta^2 + B\eta^3 + C\eta^4 = 0$$

to

$$\eta^2 (C\eta^2 + B\eta + A) = 0$$

so values of η that make the quadratic term zero are: $\eta = \{[-B \pm (B^2 - 4AC)^{1/2}]/2C\}$. For $B^2 < 4AC$, the roots are imaginary and there are no real roots. For $B^2 = 4AC$, $\eta = -B/2C$, and the situation is that of the middle curve in Fig. III-2(a). For $B^2 > 4AC$, there are two roots because of the ± of the discriminate. One root represents the upper curve in Fig. III-2(a), and the other root represents the lower curve. The important point is that the upper curve is for a temperature $T > T_t$ where the β-symmetry structure is stable and the α-symmetry structure is metastable. The middle curve is for $T = T_t$, and the two symmetries coexist in equilibrium. The lower curve is for $T < T_t$, and the β-symmetry structure is no longer stable and the α-symmetry form is the stable form. This is the situation for a first-order transition, and the inclusion of odd order terms in the Gibbs energy description will result in this situation. The structures in this case are separate phases.

Because the foregoing treatment indicates that the presence of a third-order term in the expansion of the Gibbs energy results in a first-order transition, and because the Landau rules state that odd-order terms in the definition of the Gibbs energy should be excluded, the examination of the expansion with exclusion of odd-order terms seems worthy of consideration. Such an expansion to fourth order becomes:

$$G = G^\circ + A\eta^2 + C\eta^4 \qquad \text{(Eq 1c)}$$

Plots of G-G° versus T are shown in Fig. III-2(b) for $T = T_t$ and for $T < T_t$. A curve for $T > T_t$ is not included because

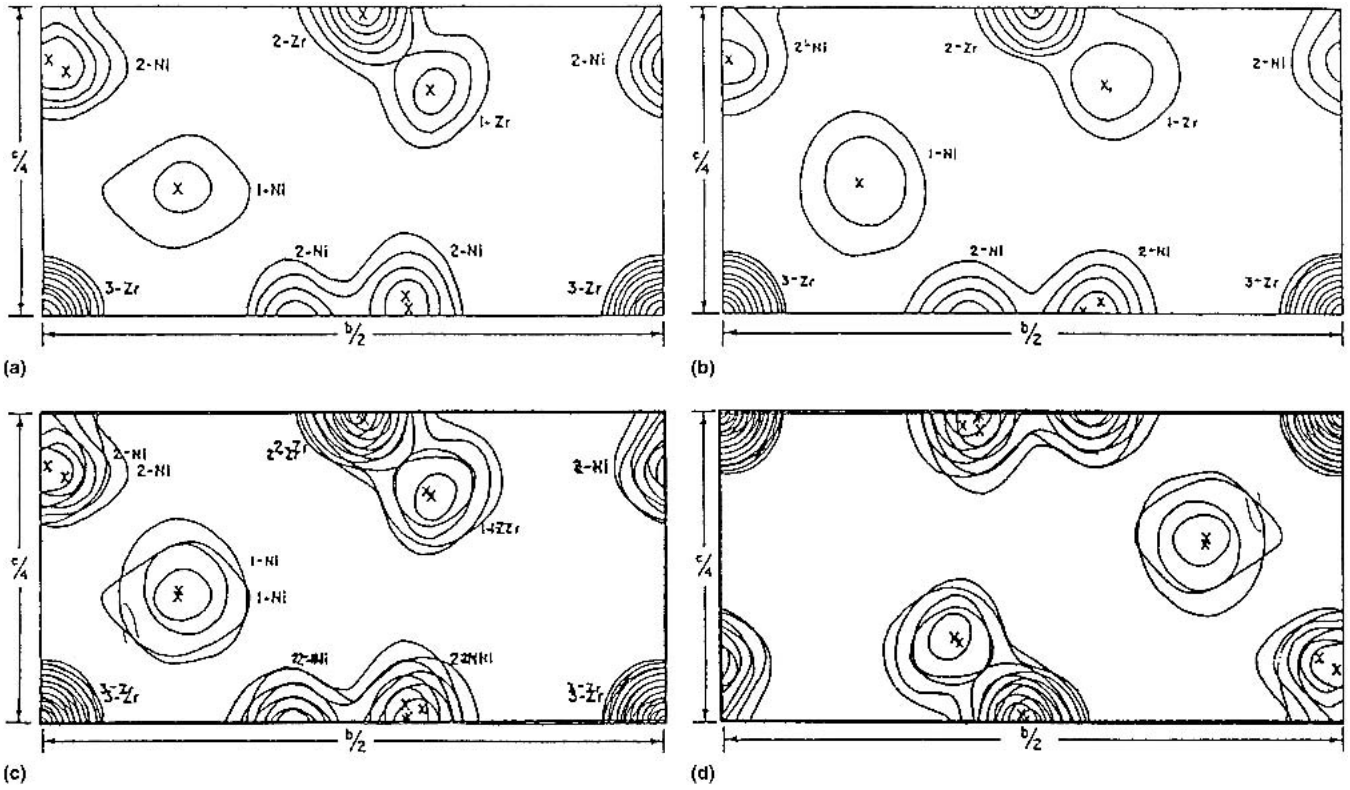

Fig. III-3 Electron density maps projected onto the *y*,*z* plane, ρ(*y*,*z*). (a) For stoichiometaric $Ni_{10}Zr_7$. (b) Zr-rich boundary of $Ni_{10}Zr_7$. (c) Superposed projections for stoichiometric and Zr-rich $Ni_{10}Zr_7$ viewed in positive **a** direction. (d) Superposed projections viewed in negative **a** direction with negative **b** and **c** directions. (c) and (d) represent the same crystal structure seen from different perspectives, but the displacement vectors in the one are the negative of the displacement vectors in the other. Note that 180° rotation of (d) becomes (c).

the two forms become identical at $T = T_t$ and remain so at temperatures above T_t with $\eta = 0$. With recognition that successive derivatives are convergent, it follows that $(\delta^2 G/\delta\eta^2) > (\delta^4 G/\delta\eta^4)$ and $(1/n!) > [1/(n+1)!]$, so $A > C$. Also in the range $0 \leq \eta \leq |1|$, it follows that $\eta^4 \leq \eta^2$. Thus, $A\eta^2$ dominates the evaluation of G-$G°$ and, for positive A values, G-$G°$ is nearly parabolic upward and $\eta = 0$ defines the stable high-symmetry configuration. When temperatures drop below T_t, the value of $(\delta G/\delta\eta)$ remains zero, but the curvature $(\delta^2 G/\delta\eta^2)$ changes from positive to negative and thus defines a maximum. Below T_t, the G-$G°$ curve develops double minima that are symmetrically oriented about $\eta = 0$ such that, at any given temperature, the magnitudes of η at the two minima are equal and the values of G-$G°$ are the same. With decreasing temperature, the magnitude of η increases and G-$G°$ becomes more negative.

The existence of two minima at the same temperature with $T < T_t$ does not mean that there are two low-symmetry structures. Rather, it means that the positive and negative values of η represent the same structure when viewed from arbitrarily different choices of coordinates. To illustrate this dependence upon coordinates, stoichiometric β-brass provides a simple example. In this case with the earlier definition of η, it can be seen that if f_{Cu} is 1, $\eta = 1$ and all of the Cu atoms are at the origin site. If that is true, all of the Zn atoms must be at the body-centered sites and the structure is completely ordered. If f_{Cu} is 0 and $\eta = -1$, the structure is again completely ordered with all of the Cu atoms on the body-centered sites and all of the Zn atoms on the origin sites. One can simply change the origin site from 000 to ½½½ to show the identity of $f_{Cu} = 1$ and $f_{Cu} = 0$.

Similarly for the displacive transitions, two symmetry-breaking parameters initially seem to represent different displacements but can be shown to be identical. For instance in the case of $Ni_{10}Zr_7$, Fig. III-3(a) and (b) show electron density projections ρ(*y*,*z*) respectively, for the stoichiometric and Zr-rich $Ni_{10}Zr_7$ structures, Fig. III-3(c) shows a superposition of Fig. III-3(a) and 3(b) illustrating the displacements of the atomic loci, and Fig. III-3(d) shows the superposition with the directions of the **b** and **c** lattice parameters reversed. The latter two projections seem to be different, but they represent the same comparison of $Ni_{10}Zr_7$ structures, with the essential difference between the Fig. III-3(c) and (d) projections being a matter of perspective, with one view being a view from the positive **a** direction and other being a view from the negative **a** direction. Note that **a**, **−b**, and **−c** also form a right-hand set so those lattice parameters could have been chosen for the structure. Thus, the two figures represent the same structure with the displacement vectors appearing to point in different directions. However, the magnitudes of the displacement vectors are the same, and the directional difference is only the result of the choice of coordinates. Both Fig. III-3(c) and (d) repre-

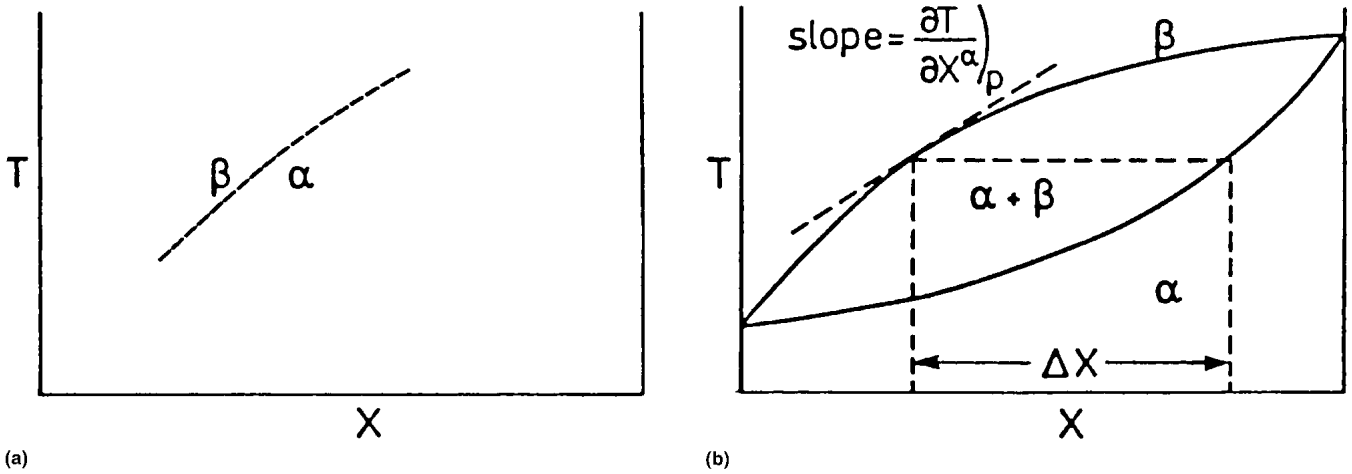

Fig. III-4 *T-X* diagrams for (a) continuous structure change and (b) two phases coexisting in equilibrium

sent the same structural differences between the stoichiometric and Zr-rich $Ni_{10}Zr_7$ structures. This illustrates that for second-order displacive transitions, as for the order-disorder transitions, it is the absolute magnitude of the η parameter that is important and not the sign.

A short word about the combined displacive, order-disorder transition would seem to be in order at this point. This is a more complicated situation, and Franzen[2] in his review article has discussed this case in some detail and has used the transition in $NaNO_2$ as an example. For those who are sufficiently interested, that reference is recommended. However, one detail of that type of this more complicated second-order transition should be noted, and that detail is that the combination of displacive distortion with order-disorder tends to destroy aspects of the long-range periodicity to produce an incommensurate lattice. This may appear as a splitting of certain diffraction maxima when the incommensurate level is low. At a higher incommensurate level, this splitting may increase to a broad blur of the maxima. However, symmetry elements of the short-range order in the structure are preserved so that all symmetry elements of the low-symmetry structure are preserved in the high-symmetry structure.

Though this author knows of no second-order transition in which all long-range order is lost, that situation would correspond to a liquid or a glass. The diffraction pattern in such an extreme incommensurate case is known as a radial distribution curve and has the general form of the angular decrease with diffraction angle Θ of an atom factor, but with a superimposed oscillatory character. This oscillatory character results from the increased electron densities from the atomic loci at atomic distances to, for instance, first-nearest neighboring atoms and second-nearest neighboring atoms.

3. Thermodynamic Functions for Second-Order Transitions

The Gibbs-Konovalow equation can be used to determine the entropy of transition for a second-order transition:

$$(\delta T/\delta X^{\alpha})_P = -\frac{\{(\delta\mu_A^{\alpha}/\delta X_A^{\alpha})_{TP} + (\delta\mu_B^{\alpha}/\delta X_B^{\alpha})_{TP}\}\Delta X}{\Delta S + (S_A^{\alpha} + S_B^{\alpha})\Delta X} \qquad \text{(Eq 2)}$$

where $(\delta T/\delta X^{\alpha})_P$ is the slope of the phase boundary of the α-structure in a temperature-composition plot, μ_A^{α} and μ_B^{α} are the partial molar Gibbs energies (chemical potentials), S_A^{α} and S_B^{α} are the partial molar entropies of the A and B components in the α-phase, and ΔX is the composition difference between the α- and β-structures at the temperature at which the slope is determined. Figure III-4 shows representative temperature-composition plots for first- and second-order transitions. Taking note of the fact that $(\delta T/\delta X^{\alpha})_P$ is finite at all compositions except at the limit of $X = 0$, there is no mathematical problem in determining a value for the slope in a first-order transition, because $\Delta X \neq 0$. However, for a second-order transition with $\Delta X = 0$ the numerator is zero, so a finite ΔS would indicate a zero slope. Thus, the only way that a finite slope could occur would be for both numerator and denominator to be zero, creating an indeterminate with a finite limit. This is an alternative way of indicating that for a second-order transition $\Delta_t S = 0$.

With $\Delta_t G = 0$ and $\Delta_t S = 0$, the relationships among Gibbs energy, entropy, and enthalpy require that $\Delta_t H = 0$. In addition, the continuity of the transition process requires that $\Delta_t V = 0$, so the question quickly comes to mind, "Is there any discontinuity in a second-order transition?" The following treatment shows that there is a discontinuity in C_p. This starts by expanding the Gibbs energy of the low-symmetry phase at temperatures in the vicinity of the transition in terms of T_t while approaching T_t from lower temperatures:

$$G = G^{\circ} + (\delta G/\delta T)_{T=T_t}(T - T_t) + \tfrac{1}{2}(\delta^2 G/\delta T^2)_{T=T_t}(T - T_t)^2 + \ldots \qquad \text{(Eq 3a)}$$

which readily converts to:

$$G = G^{\circ} - S^{\circ}(T - T_t) - \tfrac{1}{2}(C_P^{\circ}/T_t)(T - T_t)^2 + \ldots \qquad \text{(Eq 3b)}$$

where the superscript ° refers to values for the low-symmetry phase at temperatures near T_t. With recognition that G, S, and C_p of the high-symmetry structure are smoothly varying functions of temperature, it follows that, in the region of the transition at temperatures in near proximity to but below T_t, one may approximate $G \cong G°$ and $S \cong S°$. Thus, in the temperature region immediately below the transition, the Gibbs energy difference between the low-symmetry structure and the high-symmetry structure can be expressed as:

$$\Delta G = -(\Delta C_p/2T_t)(T - T_t)^2 \quad \text{(Eq 4)}$$

Thus, the excess heat capacity of the low-symmetry structure moving to the high-symmetry structure may be written as:

$$\Delta C_p = -2T_t\Delta G/(T - T_t)^2 \quad \text{(Eq 5)}$$

Because G of the low-symmetry structure is more negative than G of the high-symmetry structure at $T < T_t$, this excess heat capacity is positive. As the transition temperature is approached, ΔG should be a slowly varying function of temperature as should the C_p of the high-symmetry phase. Thus, the dominant temperature variation of the C_p of the low-symmetry structure should arise from the ratio $T_t/(T - T_t)^2$. In the immediate area of the transition, this term should increase rapidly because T_t is constant but $(T - T_t)^2$ becomes smaller as the square of the difference shrinks. One can conclude that a measurement of heat capacity should show a rapid increase at temperatures immediately below a second-order transition. To illustrate that the behavior predicted by this equation is supported by experiment, Fig. III-5 shows a plot of the heat capacity of an alloy that contains both $ThFe_3$ and Th_2Fe_7 phases, each of which has a magnetic transition.[4] The transition temperatures are, respectively, at 425 and 570 K. The nature of the transitions and the transition temperatures are corroborated by magnetic measurements.[5] Both these transitions are believed to be second order, because magnetic dipole and electric dipole transitions are dominantly second order. However, it is obvious that the λ-shape of the heat capacity of a second-order transition is very similar to the λ-shape of the heat capacity of a first-order transition so that heat-capacity measurements alone cannot uniquely distinguish a transition as being first order or second order.

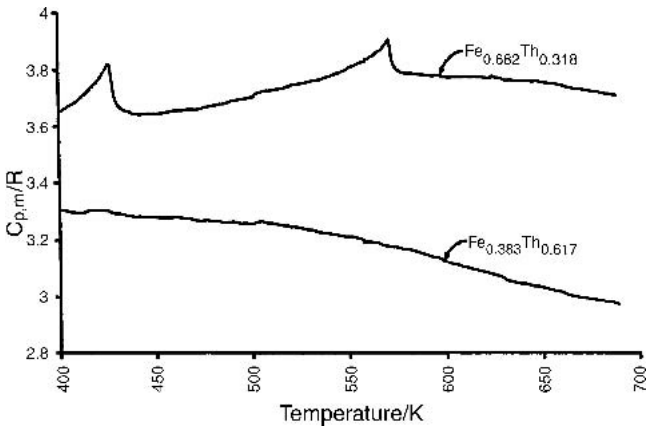

Fig. III-5 Experimental heat-capacity curves for Th-Fe alloys of 31.8 at.% Th (top curve) and 61.7 at.% Th (bottom curve). The 31.8 at.% alloy contains two ferromagnetic materials, and the two second-order magnetic transitions at 425 K for $ThFe_3$, and 570 K for Th_2Fe_7 are readily apparent. The dominant phase in the 61.7 at.% Th alloy is nonmagnetic Th_7Fe_3, and no magnetic transition is observable in that alloy.

4. Complications

While the Landau rules define the conditions that must be fulfilled before a second-order transition can occur, there is nothing in these rules that indicates the fulfillment of the conditions necessitates that an ensuing transition be second order. Indeed, in the Co-V system it has been found that the second-order magnetic transition can shift to a first-order transition. In this system, it has been found that the second-order magnetic transition in Co is initially depressed in temperature by V additions and then smoothly shifts to first order when V additions exceed a definable composition. The specifics of this transition and the general effects of magnetic transitions on phase diagrams have been discussed in detail in back-to-back articles in the same publication by Miodownik[6] and Inden.[7] Indeed, it is sometimes quite difficult to determine whether a transition is first order or second order. It has just been shown that the forms of the heat-capacity curves for first- and second-order transitions are quite similar. Hence, heat-capacity data do not uniquely characterize second-order transitions, the question arises as to how does one distinguish whether a transition is first order or second order. An example of a case in which the answer has not been resolved occurs in the alkali-nitrogen system, wherein all of the alkalis form azides with formula AkN_3. Most, but not all, of these azides undergo a crystallographic transition as temperature is varied. The crystallographic structures of both forms of NaN_3 have been determined through use of both x-ray and neutron diffraction,[8] and they are related in such a way that a continuous interchange between the structures is possible and the heat-capacity curve near the transition is λ-type. Of four studies that have investigated the nature of the transition, one[9] called it second order, another[10] called it weakly first order, and two[11,12] called it predominantly second order. Three reports[13-15] for $\Delta_t H$ gave values varying between ~0.01 and ~0.1 kJ/mol, but these indications that $\Delta_t H \neq 0$ were apparently based on the integration of heat-capacity curves and may be indicative of the energy of randomization that is distributed over a temperature range preceding the transition and thus are not a valid proof of a first-order transition.

Another interesting example of a transition wherein an obvious continuous path between two structures can occur is the tetragonal-cubic transition in In-Tl alloys. In crystallizes with a tetragonal structure that is a distortion of the face-centered cubic (fcc) closest-packed structure. The Bravais lattice of the tetragonal structure is body-centered te-

tragonal (bct), but to illustrate the close relationship with the fcc structure the body-centered lattice is frequently converted to a face-centered lattice by choosing lattice parameters $\mathbf{a}_{fc}$ and $\mathbf{b}_{fc}$, which are oriented 45° to either side of the $\mathbf{a}_{bc}$ parameter with the magnitude of $\mathbf{a}_{fc}$ and $\mathbf{b}_{fc}$ being $2^{1/2}\mathbf{a}_{bc}$. This moves atoms that were body-centered at ½½½ to face-centered positions ½½0, ½0½, and 0½½ in this alternative face-centered tetragonal (fct) lattice, the unit cell of which has a volume twice as large as the bct unit cell. A comparison of this fct unit cell with an fcc unit cell, both with one atom per lattice point, indicates that the only difference is that pure In has a **c**-to-**a** ratio of 1.076, while an fcc structure would have **c**-to-**a** ratio of 1. Addition of Tl to In produces a solid solution region in which the **c**-to-**a** ratio decreases with increasing Tl concentration to approach unity at a tetragonal-cubic transition along a boundary at 15 at.% Tl near the fusion temperature monotonically shifting to 22 to 23 at.% Tl at 0 °C. The transition is a diffusionless martensitic type that exhibits shape memory. The phase diagram was elucidated by Guttman,[13] and single-crystal elasticity studies[14,15] have shown that the compositional variation in both the tetragonal field and in the cubic field show an elastic shear constant that approaches zero. In both cases, the elastic constant is the constant associated with deformations affecting the **c**-to-**a** ratio, and a zero value for an elastic constant is the point of neutral stability, with negative values guaranteeing mechanical instability and, from the Maxwell relations, also thermodynamic instability. The question then, is "Is this a first-order or a second-order transition?"

The work of Predel[16] seems to indicate a first-order answer. Predel used a 20.45 at.% Tl alloy that transforms near room temperature, and from the cooling curve during quantitative differential thermal analysis he obtained $\Delta_t H = 0.002$ kJ/g atom. He then determined the dependence of the transition temperature upon pressure and used the Clausius-Clapeyron equation in the form $dP/dT = \Delta_t H/T\Delta V$ to obtain $\Delta V = 0.0026$ cm^3/g atom. Even though these values are miniscule, they are finite and nonzero, which indicates a first-order transformation with an extremely narrow two-phase field. Such a two-phase field has, as yet, not been experimentally observed.

5. Other Considerations

5.1 Neutron Diffraction

The utilization of diffraction data from crystal phases has a variety of uses in determining boundaries and phase fields in phase diagrams, and these have been adequately discussed in Chapter II of the initial compilation by Pearson[17] of crystallographic data. The applications noted by Pearson (e.g., phase boundary determination by the disappearing phase method or lattice parameter determination, or phases present at a given alloy composition) can be done with x-ray radiation, electron radiation, or neutron radiation. However, neutron radiation is expensive and is therefore seldom the preferred choice. There are exceptional cases in which neutron radiation has unique advantages. Such a case is the possible ordering in Pb-Tl alloys near $PbTl_3$. The entropy argument for ordering in this system is illustrated in Fig. III-6 in which experimental entropy data[18] indicate that in dilute additions of Tl into Pb the experimental curve follows the curve for ideal mixing that is indicative of random configurational entropy. However, with further Tl additions the experimental values fall below the expectations of random mixing to reach close agreement with the curve for vibrational entropy, which was calculated from the single-crystal elastic constants. Thus, the results indicate that near the composition $PbTl_3$ the experimental entropy is due solely to vibrational contributions with negligible configurational randomness. Because the atom factors of Pb and Tl differ by only one electron, the scattering power for x-rays and electrons are closely comparable so that the detection of the weak reflections that would occur from ordering are below detectable limits. The atom factors for neutrons depend upon the nuclei, and though experts say that the normal isotopic abundances for Pb and Tl result in scattering powers that also preclude the detection of ordering, such detection by neutron radiation becomes possible by isotopic enrichment of one or the other of the components. Obviously, this would make the study quite expensive, and the need for the data does not justify such an expenditure and no such experiment has been done.

Other uses for neutron diffraction are for the determination of light atoms in crystals with atoms of both light and heavy atoms and for the determination of vibrational spectra. The basis for the determination of the positions of light atoms is based on the difference in the atom factors for neutrons compared to those for x-rays or electrons. The use of neutrons for the determination of vibrational spectra rests on the fact that both the energies of diffracted neutrons and their wavelengths are commensurate with the phonons. Thus, the examination of the contours in various directions around a diffraction maxima will reflect the absorption or desorption of a quantum of phonon energy. In x-ray diffraction, the phonon energy is such a minute quantity of the energy of the x-ray photon that no significant shift is observed from the absorption or desorption of a vibrational phonon even though the wavelengths are comparable. At the other end of the spectrum, infrared radiation has the right energy relationship, so some information can be garnered from infrared spectra. However, infrared wavelengths are large with respect to phonon waves, so significant detail is lost in analyzing infrared spectra. However, for thermodynamics and phase equilibria, the Debye approximation is generally adequate, so there is little need for present purposes to elaborate on the determination of the vibrational spectra of a crystal.

5.2 Estimation of Thermodynamic Functions

In the evaluation of phase equilibria by the Calphad procedure, one frequently encounters the problem of the lack of experimental data for thermodynamic functions. Therefore, estimating procedures are useful in establishing initial values that can then be refined by Calphad evaluation. In Chapter 3 of their book, Kubaschewski and Alcock[19] propose

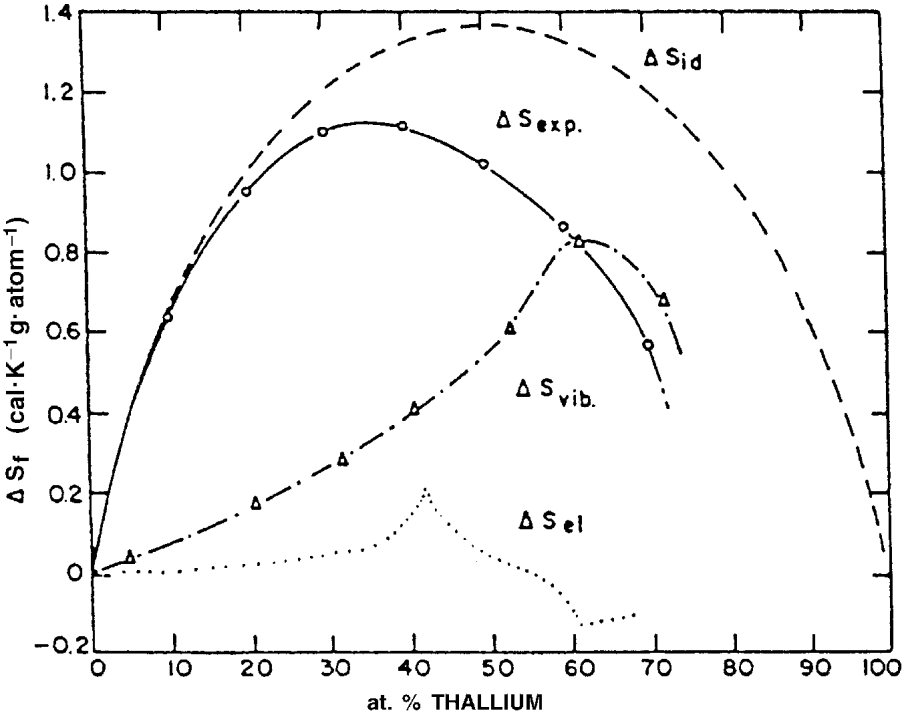

Fig. III-6 A comparison of the experimental entropy of formation with calculated contributions to illustrate a case in which neutron diffraction could be definitive in deciding whether or not atomic ordering occurs. The plots show the experimental entropy of formation (solid line) for Pb-Tl alloys, the ideal entropy of formation, which is configurational (dashed line), the vibrational contribution calculated from single crystal elastic constants (dash-dot line), and the very small electronic contribution (dotted line), which was evaluated from Fermi surface studies.

a variety of methods for estimating unknown thermodynamic quantities. These methods start by interpolating or extrapolating the trends of known values within groups or along the rows of elements of the periodic chart. Such methods are particularly useful for enthalpies of formation, $\Delta_f H$. For solids, this interpolative-extrapolative approach seems to work best when the comparisons involve related crystal structures.

A method for estimating enthalpies of phase formation not included in Chapter 3 of the book was also proposed by Kubaschewski in a separate publication.[20] This alternative estimating procedure utilizes an empirical relationship between interatomic distances in crystals, the structures of which are known and the interatomic distances in the structures of the elemental components. This approach makes no pretense of being highly precise, but in cases in which it has been tested it usually gives the correct order of magnitude. Table III-1 shows a comparison of experimental data for a series of magnesium intermetallic phases with estimates by Kubaschewski's method.[20] The comparison shows that the estimated values differ from those by experiment by as much as a factor of two. Even so, they are close enough to be useful in a computer refinement of a composite set of data for a phase diagram if no other data were available for the enthalpy of formation.

Before discussing a third method of estimating $\Delta_f H$, a digression to discuss bonding interactions seems in order. For bonding interactions, the term metal may be used to indicate those elements in which the energetically accessible orbitals (i.e., available energy states) are more numerous than the number of bonding electrons. This excess of orbitals allows a choice among a variety of hybridizations (mathematical combinations of the orbitals) to produce a close approach of a large number of atoms to one another to produce energy minimization. This bonding is, at most, weakly directional and tends to produce close-packed structures. As an example, if one packs grapefruit of a given volume with oranges of one-half that volume and the ratio of grapefruit to oranges is 1 to 2, the most efficient space filling will be a Laves structure typified by $MgCu_2$, $MgZn_2$, or $MgNi_2$. These grapefruit in such structures have 16 contiguous neighbors, whereas the closest packing of only grapefruit have only 12 contiguous neighbors. Thus, the bonding in metallic structures tends to depend upon space filling and tends to be energetically low, albeit larger as more electrons participate in the bonds, that is, the $\Delta_f H$ of the Laves phase $CaMg_2$ should be (and is) rather more negative than that of the Laves phase KNa_2 because twice as many electrons participate in the bonding in the case of $CaMg_2$.

At the other extreme is ionic bonding where $\Delta_f H$ is dominated by the coulombic attraction between positive and negative charges. The attractive interaction between any periodic charge array is easily calculated with an Ewald[21] summation as the sum of three terms or less. Coalescence of the charges is prevented by short-range repulsive interactions that increase rapidly with decreasing interionic distance. A Born-Mayer[22] potential has often been used to

Table III-1 A comparison of estimates of the enthalpies of formation by Kubaschewski's method with values determined by differing techniques for a group of binary metallic compounds of Mg

Compound	Exp. (vapor pressure Knudsen method), kJ/g-atom	Exp. (combustion calorimetry), kJ/g-atom	Exp. (vapor pressure gas transport method), kJ/g-atom	Exp. (H_2 vapor method), kJ/g-atom	Estimate (Kubaschewski method), kJ/g-atom
Mg_2Ca	12 ± 4	10 ± 3	…	8-12	18
$MgCu_2$	7.5 ± 1.7	…	…	…	16
Mg_2Cu	5.4 ± 2.5	…	…	…	2.5
$MgNi_2$	18 ± 2	16 ± 7.5	26	…	24
Mg_2Ni	22 ± 3	…	20	…	4.2
MgY	12 ± 3	…	…	…	11

Note: Exp., experimental

calculate this repulsion. A point-charge approximation for the ionic charges in this approach is justified to the extent that a spherical charge distribution acts on an external point as if it were a point charge at the sphere center. Directionality in ionic bonding is minimal as is the directionality in metallic bonding. Thus, it is not surprising to find analogous crystal structure types in both (e.g., CsCl and β-brass are isostructural). However, the $\Delta_f H$ for ionic structures tends to be at least an order of magnitude more negative than that for a metallic structure. In the Kubaschewski-Alcock[19] book, an approximation for ionic compounds can be made from the electronegativities of the ionic species with the empirical relationship:

$$\Delta_f H = -94.995 z(\varepsilon_A - \varepsilon_B)^2 \text{ kJ/mol} \quad \text{(Eq 6)}$$

where ε_A and ε_B are the electronegativities of the two species, and z is the number of valency links between the two species.

An intermediate type of bonding, is covalent bonding, wherein the number of bonding electrons is sufficient to fill the available orbitals. This type of bonding is strongly directional. Each orbital can accept two electrons, and $\Delta_f H$ tends to be intermediate between metallic and ionic. The bonding geometry is determined by linear combinations of atomic orbitals to construct molecular orbitals. Group IVA elements can be taken as an example. For C, Si, and Ge, the occupied atomic orbitals are one *s* and three *p* orbitals. These can be combined to form sp^3 orbitals, which are lobed to produce electron densities along directions aimed toward corners of a tetrahedron. Each such orbital can overlap a similar orbital from a neighboring atom to form a pair bond that is filled by an electron from the parent atom and an electron from the neighboring atom. The resultant structure has four nearest-neighbor atoms at the corners of a tetrahedral coordination and is the diamond structure with an atom at 000 and at ¼,¼,¼, plus face-centering translations of both atoms. This lattice can be duplicated in compounds. Examples are NaIn and NaTl wherein the anionic components form diamond sublattices with Na atoms filling the open spaces in the diamond structure. The rationale for producing this result is that the electron from a Na atom is loosely held, so over a time average the Na valence electron spends most of its time associated with the In or Tl sublattice, thus allowing the trivalent In or Tl atoms to utilize four electrons each in sp^3 orbitals to form a sublattice with the diamond structure. A number of references[23-25] have discussed this general type of bonding to point out the role of molecular orbital theory in crystal structures, and they have concluded that the anion sublattice dominates the resultant crystal structure. Covalent bonding also occurs to form molecules with crystals forming from molecules due to higher-order interactions such as dipole-dipole, dipole-quadrupole, or quadrupole-quadrupole. Thus, intramolecular bonding is much stronger than intermolecular bonding, so that molecular crystals tend to melt at lower temperatures, but the molecules themselves persist to quite elevated temperatures. Life itself depends on this type of bonding, and muscle contraction is a go/no-go situation and is a recrystallization under electrical stimulus.

Now, to revert to the discussion of approximating procedures, Kubaschewski and Alcock[19] have utilized the relationship between volume contraction and $\Delta_f H$ for the formation of a phase from the uncombined elements. The basis of the method is illustrated in Fig. III-7, where the dashed line represents the cohesive energy for an average of the uncombined elements and the solid line represents the cohesive energy of the combination of elements in the phase of interest. If the phase is stable, an energy reduction is expected and the attractive force interactions that lead to that energy reduction should also lead to a volume contraction with a greater contraction for a greater energy reduction. Accordingly, Kubaschewski and Alcock[19] bridged the gap across bonding types by plotting in Fig. III-8 the experimental data for the percentage volume contraction versus $\Delta_f H$ for some simple crystal structures representing a variation in bonding from primarily metallic through levels of covalency to primarily ionic. With this plot or a similar plot for other known compounds, the $\Delta_f H$ of an unknown phase can be estimated from its ΔV of formation. Such a ΔV can quite easily be determined from precision lattice parameters, density, and phase composition.

5.3 Estimation of Heat Capacities

The final item to be discussed in this review is the utilization of physical properties for the estimation of heat

capacities. Lattice vibrations are the predominant thermal energy sinks in most solids. Thus, they are of major importance to the heat capacity of a solid, and it has long been known that the temperature dependencies of the heat capacities of most solids show the same general form and, if plotted against reduced temperature, those heat capacities will fit closely to the curve of Fig. III-9. Debye approached the problem of describing the temperature dependencies of the heat capacities of solids in a manner analogous to that used by Planck to describe black-body radiation. In this approach, three basic assumptions are made. First, vibrational frequencies, ν, range between zero for infinite wavelength to a cutoff of ν_D for a high-frequency limit. The long wavelength of infinity is justified by the fact that the smallest particle that can be seen by the naked eye contains on the order of $10^{[20]}$ atoms, so a wavelength of particle dimensions is effectively infinite with respect to the size of an atom. The short wavelength or high-frequency limit can be inferred from the realization that for wavelengths shorter than twice the interatomic spacing there is nothing to vibrate. The second assumption is that all directions in a solid are equivalent. This is not rigorously correct for a crystal but is not unreasonable for randomly oriented grains in a polycrystalline solid, and, even for a single crystal, experimental evidence indicates that the assumption is acceptable. The third assumption is a neglect of dispersion in that all longitudinal waves are assumed to travel with the same single velocity, $v_L = \nu\lambda$, and all shear waves were assumed to travel with a single, but different, velocity, $v_S = \nu\lambda$, so that frequency, ν, and wavelength, λ, are inversely related for the entire vibrational spectrum.

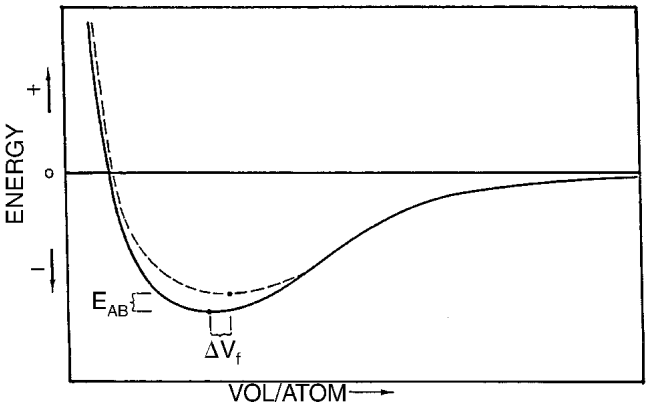

Fig. III-7 Schematic curves for cohesive energies (enthalpies of sublimation at 0 K) such as might be calculated from first principles. The O value represents the state in which individual atoms are infinitely separated. The dashed curve represents the average of the component elements at the ratio of the phase composition and the solid line represents the stable phase. The difference in the depths of the minima represents the binding energy, and the energy reduction producing phase stability should also lead to a volume contraction. Note that the curvature at the minima is a measure of the bulk moduli.

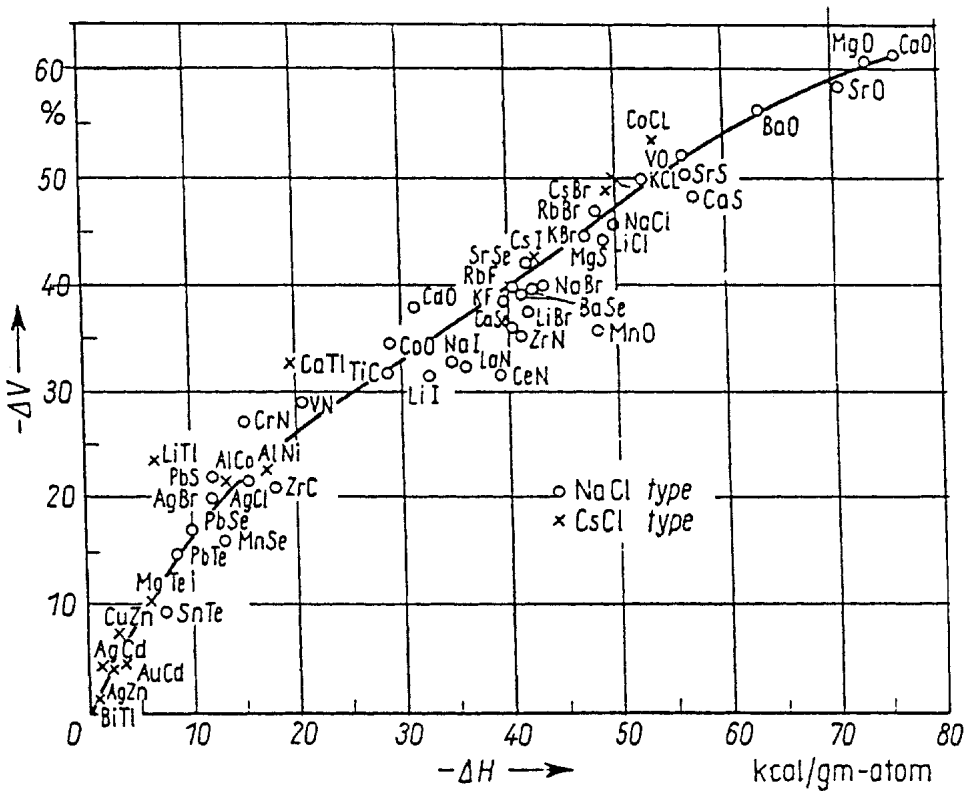

Fig. III-8 A plot of the percentage volume contraction versus heats of phase formation per g-atom for a variety of materials with the composite data showing a well-defined trend (after Kubaschewski and Alcock[19]).

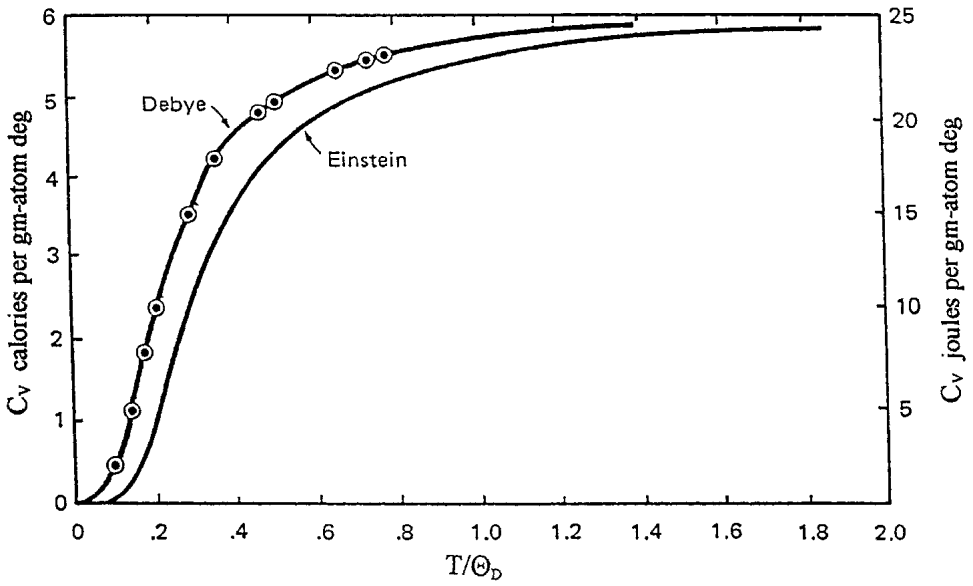

Fig. III-9 Constant volume heat capacity versus reduced temperature for a Debye model and for an Einstein model. The points on the Debye curve are representative of Table III-2.

Then with three degrees of freedom for each atom and quantum statistics (phonon-photon statistics) for the probability of excitation of the vibrational modes, Debye derived the following relationship for the evaluation of the heat capacity, C_v:

$$C_v = 9R(T/\Theta_D)^3 \int_0^{\Theta_D/T} x^4 e^x (e^x - 1)^{-2}\, dx \qquad \text{(Eq 7)}$$

where $x = h\nu/kT$ with h being Planck's constant, k being the Boltzmann constant, and kT being the thermal energy available for partition to a vibrational mode. The cutoff limit for x_{max} is the upper frequency limit $h\nu_D/kT$, which is equivalent to Θ_D/T because $h\nu_D = k\Theta_D$. The evaluation of Eq 7 for various temperatures produces the values of C_v shown in Table III-2. Note that in the tabulation temperature increments are smaller in the low-temperature region than in the high-temperature region. This is because in the temperature range $0 < T < \Theta_D$, the kT energy is inadequate to activate high-frequency vibrational modes having $h\nu > kT$. For $T > \Theta_D$, a plateau is reached and all modes are activated, and heat additions serve only to increase vibrational amplitudes. Because differential internal energy, $dE = C_v dT$, and differential entropy, $dS = C_v d \ln T$, Eq 2 can be modified to produce equations for evaluations of E and S at selected temperatures, and tabulations for these functions are shown in Tables III-3 and III-4.

Obviously corrections must be made for constant pressure processes, which for a solid takes the form:

$$C_p - C_v = VT\alpha_V^2 \kappa \qquad \text{(Eq 8)}$$

where α_V is the volume coefficient of expansion ($3\,\alpha_L$) and κ is the bulk modulus or reciprocal compressibility. In addition, it should be emphasized that the values in Tables III-2 to 4 represent only the vibrational contributions, and any other heat-capacity sink needs to be considered. However, the heat capacities of a large majority of solids arise predominately from heat absorption by vibrational modes. Einstein's early work on heat capacities also used phonon-photon statistics for the excitation of vibrational modes, but assumed a mean characteristic frequency that was constant for all atoms. The resulting difference in predicted heat capacity values is apparent in Fig. III-9.

To use the tabulated values, one must first have an evaluation of Θ_D. To determine a value for Θ_D, one may take advantage of the fact that many physical properties are affected by lattice vibrations, for example, electrical resistivity of metals, elasticity, and hardness. In the case of electrical resistivity, a correlation with lattice vibrations is expected because the electrons in a crystal are in states that satisfy the potential field of the periodic lattice. Thus, any extraneous potential will tend to scatter an electron from its occupied state to another state. Thus, extraneous potentials are induced by vibrations as atoms are displaced from their equilibrium locations. However, any imperfection in the crystal structure will also act as a scattering center with point imperfections in the form of vacancies, foreign atoms, and interstitials being the most important. However, these imperfections are not temperature-sensitive, and their contribution can be abstracted by subtracting the residual resistivity at low temperature from experimental resistivities to determine ρ_T values.

Then ρ_T/T values can be plotted against temperature to find a value of Θ_D, which reduces the plot to agree with a plot of the C_v values in Table III-3. Determinations of Θ_D that are made in this manner are generally in good accord (within ~10 K) with values determined by heat-capacity measurements. Electrical resistivity measurements are rela-

Table III-2 Values of C_v evaluated at various values of Θ_D/T with Eq 7

Θ_D/T	0.00	0.01	0.02	0.03	0.04	0.05	0.06	0.07	0.08	0.09
0.1	5.733	5.710	5.688	5.667	5.646	5.625	5.604	5.583	5.562	5.541
0.2	5.520	5.500	5.480	5.459	5.438	5.417	5.396	5.375	5.354	5.333
0.3	5.312	5.291	5.271	5.250	5.230	5.210	5.190	5.170	5.150	5.130
0.4	5.110	5.091	5.071	5.051	5.031	5.012	4.992	4.972	4.952	4.933
0.5	4.913	4.893	4.874	4.855	4.836	4.817	4.788	4.779	4.760	4.741
0.6	4.722	4.704	4.685	4.666	4.647	4.628	4.610	4.592	4.574	4.555
0.7	4.536	4.518	4.500	4.483	4.465	4.447	4.429	4.412	4.394	4.376
0.8	4.358	4.341	4.324	4.307	4.290	4.273	4.255	4.238	4.221	4.203
0.9	4.186	4.169	4.152	4.135	4.118	4.101	4.084	4.067	4.050	4.033
1.0	4.017	4.001	3.985	3.968	3.952	3.935	3.918	3.902	3.886	3.870
1.1	3.854	3.838	3.822	3.806	3.790	3.774	3.758	3.742	3.726	3.710
1.2	3.695	3.680	3.665	3.650	3.635	3.620	3.605	3.590	3.575	3.560
1.3	3.545	3.530	3.515	3.500	3.486	3.471	3.457	3.442	3.428	3.413
1.4	3.399	3.385	3.371	3.357	3.343	3.329	3.315	3.301	3.287	3.273
1.5	3.259	3.245	3.231	3.217	3.203	3.190	3.176	3.163	3.150	3.136
1.6	3.123	3.110	3.096	3.082	3.069	3.056	3.043	3.030	3.017	3.004
1.7	2.992	2.979	2.966	2.953	2.940	2.927	2.915	2.902	2.890	2.877
1.8	2.864	2.851	2.839	2.826	2.814	2.801	2.789	2.776	2.764	2.752
1.9	2.739	2.727	2.716	2.704	2.692	2.681	2.670	2.659	2.648	2.637
Θ_D/T	0.0	0.1	0.2	0.3	0.4	0.5	0.6	0.7	0.8	0.9
0	5.955	5.7330	5.5195	5.3122	5.1100	4.9130	4.7220	4.5364	4.3578	4.1862
1	4.0168	3.8536	3.6951	3.5450	3.3991	3.2592	3.1229	2.9920	2.8640	2.7395
2	2.6266	2.5138	2.4068	2.3047	2.2044	2.1078	2.0166	1.9288	1.8446	1.7642
3	1.6873	1.6131	1.5423	1.4756	1.4118	1.3492	1.2917	1.2364	1.1825	1.1314
4	1.0921	1.0361	0.9931	0.9517	0.9118	0.8733	0.8361	0.8002	0.7654	0.7317
5	0.7009	0.6712	0.7438	0.6187	0.5944	0.5708	0.5478	0.5255	0.5037	0.4824
6	0.4618	0.4437	0.4259	0.4088	0.3926	0.3787	0.3652	0.3519	0.3387	0.3257
7	0.3128	0.3017	0.2908	0.2803	0.2702	0.2605	0.2513	0.2423	0.2340	0.2263
8	0.2195	0.2135	0.2077	0.2017	0.1959	0.1905	0.1855	0.1797	0.1744	0.1691
9	0.1639	0.1588	0.1536	0.1485	0.1435	0.1384	0.1336	0.1289	0.1242	0.1195
10	0.1149	0.1107	0.1070	0.1028	0.1009	0.0983	0.0957	0.0953	0.0907	0.0886
11	0.0866	0.0845	0.0824	0.0804	0.0783	0.0763	0.0742	0.0722	0.0704	0.0686
12	0.0671	0.0655	0.0640	0.0625	0.0610	0.0595	0.0580	0.0565	0.0552	0.0540
13	0.0526	0.0514	0.0502	0.0491	0.0481	0.0471	0.0461	0.0451	0.0441	0.0431
14	0.0420	0.0411	0.0403	0.0395	0.0388	0.0380	0.0373	0.0365	0.0358	0.0350
15	0.0343	0.0335	0.0328	0.0320	0.0313	0.0308	0.0303	0.0298	0.0293	0.0288

Note: Units, (Joules/4.184) per g-atom degree

tively easy to make, but abstraction of the residual resistivity requires a capability for measurement at low temperatures. The evaluation of Θ_D from resistivity data is, of course, limited to metallic conductors and precludes semiconductors wherein the number of charge carriers changes with temperature.

Elasticity is another good approach to the evaluation of Θ_D, because the atomic-force interactions within a crystal control the vibrational spectra. In this approach, the evaluation of Θ_D is made from the relationship:

$$\Theta_D = 9h^3\Omega_o/4\pi k(v_L^{-3} + 2v_S^{-3}) \quad \text{(Eq 9)}$$

where h and k are, respectively, Planck's and Boltzmann's constants, Ω_o is the volume per atom, and v_L and v_S are, respectively, the longitudinal and shear-wave velocities in a given direction in the solid. These velocities are readily derived from elastic moduli because the substitution of Hooke's law into Newton's law generates a stress-acceleration relationship that involves the square of the wave velocities and the elastic constants:

$$V_L^2 = Y(1-\sigma)/[\rho(1+\sigma)(1-2\sigma)] = 3\kappa(1-\sigma)/[\rho(1+\sigma)] \quad \text{(Eq 10a)}$$

$$V_S^2 = \mu/\rho = Y/[2\rho(1+\sigma)] = 3\kappa(1-2\sigma)/[2\rho(1+\sigma)] \quad \text{(Eq 10b)}$$

$$\sigma = [2 - (v_S^2/v_L^2)]/2[1 - (v_S^2/v_L^2)] \quad \text{(Eq 10c)}$$

Table III-3 Values of $E/T = T^{-1}\int_0^T C_v\,dT$ for various values of Θ_D/T

Θ_D/T	0.00	0.01	0.02	0.03	0.04	0.05	0.06	0.07	0.08	0.09
0.1	21.65	21.16	20.69	20.23	19.79	19.37	18.99	13.62	18.26	17.79
0.2	17.53	17.23	16.98	16.73	16.47	16.22	15.97	15.74	15.52	15.31
0.3	15.12	14.93	14.76	14.59	14.42	14.25	14.08	13.91	13.74	13.58
0.4	13.42	13.27	13.13	13.00	12.86	12.73	12.60	12.47	12.35	12.22
0.5	12.08	11.98	11.86	11.75	11.64	11.53	11.41	11.32	11.22	11.12
0.6	11.03	10.93	10.84	10.75	10.63	10.56	10.47	10.38	10.29	10.21
0.7	10.14	10.04	9.96	9.88	9.80	9.73	9.66	9.58	9.51	9.45
0.8	9.364	9.291	9.229	9.162	9.094	9.027	8.959	8.892	8.825	8.756
0.9	8.689	8.630	8.564	8.495	8.440	8.379	8.320	8.263	8.208	8.150
1.0	8.094	8.039	7.984	7.928	7.873	7.818	7.762	7.707	7.653	7.601
1.1	7.549	7.498	7.447	7.396	7.346	7.302	7.249	7.201	7.153	7.105
1.2	7.060	7.015	6.970	6.925	6.580	6.835	6.791	6.748	6.706	6.663
1.3	6.621	6.579	6.537	6.496	6.455	6.413	6.373	6.333	6.295	6.256
1.4	6.218	6.185	6.144	6.107	6.069	6.032	5.995	5.958	5.921	5.885
1.5	5.849	5.813	5.778	5.743	5.709	5.675	5.640	5.607	5.574	5.540
1.6	5.507	5.475	5.442	5.410	5.379	5.347	5.316	5.285	5.253	5.222
1.7	5.191	5.160	5.130	5.100	5.070	5.041	5.012	4.982	4.953	4.924
1.8	4.895	4.867	4.840	4.811	4.783	4.755	4.728	4.700	4.672	4.645
1.9	4.617	4.590	4.565	4.539	4.513	4.488	4.463	4.438	4.414	4.390
Θ_D/T	0.0	0.1	0.2	0.3	0.4	0.5	0.6	0.7	0.8	0.9
0	…	21.6510	17.5293	15.1233	13.4213	12.1051	11.0354	10.1357	9.3643	8.6892
1	8.0934	7.5484	7.0601	6.6206	6.2183	5.8491	5.5068	5.1906	4.8947	4.6176
2	4.3680	4.1296	3.9084	3.7020	3.5055	3.3202	3.1484	2.9861	2.8332	2.7493
3	2.5538	2.4253	2.3042	2.1913	2.0849	1.9816	1.8871	1.7976	1.7115	1.6306
4	1.5529	1.4810	1.4141	1.3502	1.2892	1.2309	1.1750	1.1214	1.0698	1.0202
5	0.9748	0.9317	0.8914	0.8548	0.8195	0.7854	0.7525	0.7206	0.6897	0.6595
6	0.6306	0.6050	0.5799	0.5562	0.5334	0.5138	0.4950	0.4765	0.4583	0.4403
7	0.4225	0.4072	0.3922	0.3777	0.3639	0.3506	0.3381	0.3258	0.3144	0.3033
8	0.2946	0.2865	0.2786	0.2704	0.2626	0.2351	0.2484	0.2406	0.2334	0.2263
9	0.2193	0.2124	0.2054	0.1985	0.1918	0.1850	0.1785	0.1722	0.1659	0.1596
10	0.1535	0.1478	0.1428	0.1386	0.1347	0.1312	0.1277	0.1242	0.1210	0.1182
11	0.1155	0.1127	0.1099	0.1072	0.1044	0.1017	0.0989	0.0963	0.0939	0.0915
12	0.0895	0.0873	0.0853	0.0833	0.0813	0.0793	0.0773	0.0753	0.0736	0.0720
13	0.0701	0.0686	0.0669	0.0655	0.0641	0.0628	0.0615	0.0601	0.0588	0.0575
14	0.0560	0.0548	0.0537	0.0527	0.0517	0.0506	0.0497	0.0487	0.0477	0.0467

Note: Units, (Joules/4.184) per g-atom

In these equations, Y is Young's modulus, μ, is the shear modulus, κ is the bulk modulus or reciprocal compressibility, ρ is the density, and σ is Poisson's ratio. This assumes that measurements of the moduli were made on a polycrystalline aggregate with random grain orientation so that all directions are equivalent. In that case, any two of the moduli are adequate for the determination of the sonic velocities and thence of Θ_D. In the rare event that the elastic constants for single crystals of the material of interest are available, conversion of these constants to a Θ_D with the Debye approximation has been discussed by Anderson[27] and with the Born-van Karman method by de Launay.[28] The latter includes specific consideration of directional variation of the sonic velocities but still neglects dispersion.

If no elasticity data are available, an estimate of the bulk modulus can be made on the basis that compressibility is primarily an atomic function. The compressibility is $\beta = -V(\delta P/\delta V) = 1/\kappa$ and, because $\delta E/\delta V = -P$, $\beta = V(\delta^2 E/\delta V^2)$. This means that in Fig. III-7 the curvature of the two curves at the minima are, respectively, the weighted compressibilities of the two components and of the intermediate phase. Then, if the cohesive energy of the phase is written as the weighted sum of the cohesive energies of the components plus an energy reduction for stability:

$$E_P = X_A E_A + X_B E b_B + E_{AB} \qquad \text{(Eq 11)}$$

it follows that:

$$\beta_P = \beta_A + \beta_B + V(\delta^2 E_{AB}/\delta V^2) \qquad \text{(Eq 12)}$$

The argument is that with small ΔE and ΔV the last term is likely to be small so that the additivity of the compressibili-

Table III-4 Values of $S = \int_0^T (C_v/T)\, dT$ for various values of Θ_D/T

Θ_D/T	0.0	0.1	0.2	0.3	0.4	0.5	0.6	0.7	0.8	0.9
0	5.955	5.95	5.94	5.93	5.91	5.88	5.85	5.81	5.77	5.72
1	5.670	5.61	5.55	5.48	5.41	5.34	5.26	5.18	5.09	5.01
2	4.918	4.83	4.74	4.64	4.54	4.45	4.35	4.25	4.15	4.05
3	3.948	3.85	3.75	3.65	3.56	3.46	3.36	3.27	3.18	3.09
4	2.996	2.91	2.82	2.74	2.65	2.57	2.50	2.42	2.34	2.27
5	2.197	2.13	2.06	1.99	1.93	1.87	1.81	1.75	1.69	1.63
6	1.582	1.53	1.48	1.43	1.39	1.34	1.30	1.26	1.21	1.18
7	1.137	1.100	1.065	1.031	0.998	0.966	0.935	0.906	0.878	0.850
8	0.823	0.798	0.774	0.750	0.727	0.704	0.683	0.662	0.642	0.623
9	0.604	0.588	0.570	0.552	0.537	0.521	0.507	0.492	0.478	0.465
10	0.452	0.439	0.427	0.415	0.404	0.394	0.383	0.373	0.363	0.353
11	0.345	0.335	0.324	0.319	0.310	0.303	0.295	0.287	0.280	0.273
12	0.267	0.260	0.254	0.248	0.242	0.237	0.231	0.226	0.221	0.216
13	0.211	0.206	0.202	0.197	0.193	0.188	0.184	0.180	0.176	0.172
14	0.169	0.165	0.162	0.159	0.155	0.152	0.149	0.146	0.143	0.140
15	0.137	0.135	0.132	0.130	0.127	0.125	0.122	0.120	0.118	0.116

Θ_D/T	C	Θ_D/T	C	Θ_D/T	C
16	0.113	21	0.0502	26	0.0264
17	0.0945	22	0.0436	27	0.0236
18	0.0796	23	0.0382	28	0.0212
19	0.0677	24	0.0336	29	0.0190
20	0.0581	25	0.0298	30	0.0172

Note: Units, (Joules/4.184) per g-atom degree Source: Ref 26.

ties or bulk moduli is likely to be a good approximation. Thus, one elastic modulus can be evaluated solely from elemental data. A second estimate for Poisson's ratio can be made from the fact that a large majority of values for that ratio have been reported to fall between 0.25 and 0.35. An estimate of 0.3 is therefore likely to be valid within 16%.

In conclusion, it can be said that there are other methods of approximating the Debye temperature, but in most cases they tend to be less reliable. One can certainly be more sophisticated and consider that the vibrational modes consist of an acoustical branch (all atomic species move for the most part in phase) and one or more optical branches (unlike atomic species move out of phase), depending upon the number of kinds of atoms in the crystalline structure. In that case, one might treat the acoustical branch with a Debye model and each optical branch with an Einstein model. However, except in the case of large mass differences between atomic species, the effort involved would hardly be worthwhile. For example, in the case of β-brass there is only one unit difference in mass, and the energy gap between the branches is negligible.

References

1. L. Landau and E. Lifshitz, *Statistical Physics,* Pergamon Press, 1959, p 430-456
2. H.F. Franzen, *Lecture Notes in Chemistry* Vol 32, *Second Order Phase Transitions and the Irreducible Representation of Space Groups,* Springer Verlag, 1982
3. V. Heine and J.D.C. McConnell, *Phys. Rev. Lett.,* Vol 46, 1981, p 1092
4. F.C. Laabs, M.A. Noack, and J.F. Smith, *J. Phase Equilibria,* Vol 12, 1991, p 23
5. K.H.J. Buschow, *J. Appl. Phys.,* Vol 42, 1971, p 3433
6. A.P. Miodownik, *Bull. Alloy Phase Diagrams,* Vol 2 (No. 4), 1982, p 406
7. G. Inden, *Bull. Alloy Phase Diagrams,* Vol 2 (No. 4), 1982, p 412
8. J. Sangster, *J. Phase Diag. Diff.,* Vol 25, 2004, p 560
9. W. Carling and E.F. Westrum, *J. Chem. Thermodyn.,* Vol 8, 1976, p 565
10. S.R. Aghdee and A.I.M. Rae, *J. Chem. Phys.,* Vol 79, 1983, p 4558
11. E. Pringle and D.E. Noakes, *Acta Crystallogr.,* Vol B24, 1968, p 262
12. S.R. Aghdee and A.I.M. Rae, *Acta Crystallogr.,* Vol B40, 1984, p 214
13. L. Guttman, *Trans. Am. Min. Met. Eng.,* Vol 13, 1950, p 381
14. N.G. Pace and G.A. Saunders, *Philos. Mag.,* Vol 22, 1970, p 73
15. D.B. Novotny and J.F. Smith, *Acta Metall.,* Vol 13, 1965, p 381
16. B. Predel, *Z. Metallkde,* Vol 55, 1964, p 117
17. W.B. Pearson, *Handbook of Lattice Spacings and Structures of Metals and Alloys,* Pergamon Press, NY, 1958, Chap. II
18. M.L. Shepard and J.F. Smith, *Acta Metall.,* Vol 15, 1967, p 357

19. O. Kubaschewski and C.B. Alcock, *Metallurgical Thermochemistry,* 5th ed., Pergamon Press, Oxford, 1979, Chap. III
20. O. Kubaschewski, *The Physical Chemistry of Metallic Solutions and Intermetallic Compounds,* Her Majesty's Stationery Office, London, 1959, Vol 1, Paper 3C
21. P.P. Ewald, *Ann. Phys.,* Vol 64, 1921, p 253
22. M. Born and J.E. Mayer, *Z. Phys.,* Vol 73, 1932, p 1
23. J.D. Corbett and R.E. Rundle, *Inorganic Chem.,* Vol 3, 1964, p 1408
24. W.B. Pearson, *Acta Crystallogr.,* Vol 17, 1964, p 1
25. A. Kjekshus, *Acta Chem. Scand.,* Vol 18, 1966, p 2379
26. *Handuch der Physik,* Vol 10, p 367
27. O.L. Anderson, *J. Phys. Chem. Solids,* Vol 24, 1963, p 909
28. J. de Launay, *Solid State Physics,* F. Seitz and D. Turnbull, Ed., Academic Press, 1956, Vol 2, p 276-284